Quantitative Biofractal Feedback Part II

"Devices, Scalability & Robust Control"

Robert L. Ewing, PhD
Air Force Research Laboratory
Wright Patterson Air Force Base
Information Directorate, AFRL/RITA, Bldg 620
Dayton, Ohio 45433

robert.ewing@wpafb.af.mil

ABSTRACT

Development of a new revolutionary quantitative biofractal control methodology for the creation and efficient use of new organic bio-inspired devices using quantitative feedback theory (QFT) will be the focus of this lecture. The non-integer methodology will be addressed in the form of a quantitative biofractal controller architecture, which incorporates ontogentic and epigenetic scalable mechanisms for interconnectivity parameter weightings, morphability and dimensional scalability in the development of nonlinear sensor models and methodology. Quantitative feedback for biofractal devices requires that a higher temporal and/or spectral models become available at the system level to implement a precision, low power, low weight integrated real-time sensor for mobile platforms applications such as unmanned air vehicles, emerging optical communication and application of organic device applications for multifunctional low power sensor for optical and RF.

Why biofractal? Biofractal involves the used of organic devices, where power, size and cost are the driving metrics for the use of this new technology. Organic devices couples the multiphysics effects of ionics and electronics, with feedback involving additional complicating factors using fractal quantitative feedback technique in areas of multiple signal carriers and fragility.

(1) Multiple signal carriers. We will explore the use of organic ionic flow devices for biofractal modelling. In contrast, digital electronics employs only one signal carrier, i.e., the electron. Current and voltage signals are simply different views of electron flow. Even the positive "hole" flow found in semiconductors consists simply of electrons moving in reverse, and may be modelled as such. Ionic devices, however, will employ multiple signal types. In addition to electric and light signals, there are ions and molecules that serve as signals by participating in chemical reactions. Such species have unique behavior that varies with chemical context. Unlike electrons, they must maintain their unique multiphysics identities when modelled.

(2) Fragility. Organic devices are less robust than semiconductors, able to endure fewer environmental extremes. This fragility can translate into less reliability, and necessitate redundancy, dimensional scalability and error-correction techniques on a scale greater than in silicon processing. Such introduced complexity requires the application of QFT's robustness.

The advantage of using QFT is the ability to synthesize the fractional control circuits targeting nonlinear

Report Documentation Page

Form Approved
OMB No. 0704-0188

1. REPORT DATE	2. REPORT TYPE	3. DATES COVERED
MAY 2008		**00-00-2008 to 00-00-2008**

4. TITLE AND SUBTITLE	5a. CONTRACT NUMBER
Quantitative Biofractal Feedback Part II 'Devices, Scalability & Robust Control'	5b. GRANT NUMBER
	5c. PROGRAM ELEMENT NUMBER
6. AUTHOR(S)	5d. PROJECT NUMBER
	5e. TASK NUMBER
	5f. WORK UNIT NUMBER
7. PERFORMING ORGANIZATION NAME(S) AND ADDRESS(ES) **Air Force Research Laboratory,Information Directorate, AFRL/RITA,Wright Patterson AFB,OH,45433**	8. PERFORMING ORGANIZATION REPORT NUMBER
9. SPONSORING/MONITORING AGENCY NAME(S) AND ADDRESS(ES)	10. SPONSOR/MONITOR'S ACRONYM(S)
	11. SPONSOR/MONITOR'S REPORT NUMBER(S)

12. DISTRIBUTION/AVAILABILITY STATEMENT
Approved for public release; distribution unlimited

13. SUPPLEMENTARY NOTES
See also ADM002223. Presented at the NATO/RTO Systems Concepts and Integration Panel Lecture Series SCI-195 on Advanced Autonomous Formation Control and Trajectory Management Techniques for Multiple Micro UAV Applications held in Glasgow, United Kingdom on 19-21 May 2008.

14. ABSTRACT
See Report

15. SUBJECT TERMS

16. SECURITY CLASSIFICATION OF:			17. LIMITATION OF ABSTRACT	18. NUMBER OF PAGES	19a. NAME OF RESPONSIBLE PERSON
a. REPORT	b. ABSTRACT	c. THIS PAGE			
unclassified	**unclassified**	**unclassified**	**Same as Report (SAR)**	**26**	

sensors and devices. But controllability is really the problem area in the biofractal controller design in terms of reliability, lack of CAD tools, and robust performance issues. So, the QFT robust design methodology needs to be enhanced for simulation ,modelling and synthesis of robust "scalable" biofractal feedback designs. The envisioned robust biofractal circuit design methodology involves the decomposition of the performance specifications into the basic Op-Amp building blocks, such as an integrator and summer, correlated to fractal elements. The inherent basic elements used for the Op-Amp building blocks will be both novel organic transistors and silicon devices. Novel organics have good potential for development of unique multi-signal logic devices that don't rely on conventional electronic designs. Compared to the electrons and holes in their semiconductor counterparts, organic transistors utilize charge carriers such as electrolytes to conduct a signal. This provides the potential for custom biofractal logic built around device chemistry that can lead to reduced complexity in intricate logic implementations.

1.0 INTRODUCTION

Stop thinking that the universe is best described by integer derivatives, it is not. Even Newton's law, can be decomposed into fractal components. The overall advantage is that fractal transfer functions can characterize complex nonlinear dynamics, with only a few parameters in contrast to integer expressions, that even with 10X or more parameters, still do not fully model the physical phenomena The 1970's started research in ionic chemical sensors, know as CHEMFETs. It was with the realization that the use of half-order derivatives and integrals led to the formation of 3-D physical geometric designs that could be modelled in a closed form solution. These half-order fractal expressions required only a parametric gain constant variation between rectangular and spherical coordinates which were more functional and less complex then Fick's laws of diffusion [1]. The difficult implementation aspects for noninteger fractals have been known for over a hundred years. Isaac Newton was said to get headaches thinking about the 3-body problem (Sun, Moon, and Earth). There are several reasons for the 3D modelling, and hence the complexity of the calculations. First, is in attempting to increase the accuracy and complexity of the representations of the physical conservation laws. For example, in chemical models, increasing the number of chemical species considered increases the number of dependent variables. The obvious need for increased independent variables comes from the need to represent the sensor phenomena in two and three spatial dimensions. However, even higher dimensional problems arise when the independent variables are not the spatial coordinates but are various state descriptions; such as higher-dimensional problems are common in physics and chemistry. Unfortunately, the direct applications of numerical methods that work well in one or two dimensions often are not usable in three dimensions. Therefore, increasing the degrees of freedom related to 3D modelling, requires non-integer derivation, where it has already been used to correctly model the diffusion phenomenon of magnetic field in electrical machines [2] which is a physical phenomenon similar to one found in the electrochemical devices. The resulting parameters of such non-integer order models have a close link with the physical characteristics of the system and are precise, having less number of parameters and being valid on a wide frequency range. Moreover, this method is very useful for the optimal real-time control of scaleable sensors, if dimensional analysis techniques are used in the models.

1.1 Fractal Control Feedback

The first mention of the interest of considering a fractal differential operator in a feedback loop, though without mention of the term "fractal", was made by Bode [3], and later in more comprehensive way in [4]. A key problem in the design of a feedback amplifier was to come up with a feedback loop so that the performance of the closed loop was invariant to changes in the amplifier gain. Bode presented an elegant solution to this robust design problem, which he called the ideal cutoff characteristic. Bode's idea to stabilize control, by the use of loop shaping to design controllers that are insensitive to gain variations was later

generalized by Horowitz to systems that are insensitive to gain and phase variations of the plant, culminating in the Quantitative Feedback Theory method [5].

1.2 Dimensional Analysis for Biofractal Models (*Buckingham's Theorem)*

It's important to develop scalable performance biofractal models for complex multiphysics systems. Dimensional analysis[6,8] provides the key to insight for telling us how the numerical value of a quantity changes when the basic units of measurement are subjected to prescribed changes. It has been very successful for fluidic modelling, and thus will be an invaluable tool for the "scalable" biofractal models and organic ionic devices. It has its beginnings with Maxwell (1871), the Scottish physicist who used symbols of the type [F], [M], [L], [T], [ϕ] to denote force, mass, length, time, and temperature, respectively. The dimensions of these physical quantities can be manipulated algebraically and the results can be interpreted to provide information about the physical processes involved in the scaling process. The fundamental theorem of dimensional analysis is: *If an equation is dimensionally homogenous it can be reduced to a relationship among a complete set of dimensionless products of the system variables, or also know as Buckingham's Theorem.* The dimensionless products are called Π terms. These terms do not depend on the fundamental units of measurement. The set of dimensionless products is complete when each product is independent and any other dimensionless product that can be formed from the variables is a product of the pi terms in the set. This proposes the following questions of: How many dimensionless products form a complete set? How are the dimensionless products formed? These questions will be answered by looking at the following two examples (Sections 1.2.1-1.2.3).

1.2.1 Microfluidic Scaling Example [8,12]

To give some insight to dimensionless products, lets consider a microfluidic example[8]. The first step is to list all the variables that are involved in the phenomenon. Suppose the drag force, F, on a smooth body, in a stream of incompressible fluid with a relative velocity, v, body diameter, D, mass density of fluid, ρ, and viscosity of fluid, ν, is to be found. So, we have the variables F, v, D, ρ, ν. The dimensionless term will have the form:

$$\pi = F^a v^b D^c p^d \nu^e \qquad (1.1)$$

where the literal constants *a* to *e* must be determined.

Since π is dimensionless, then:

$$\begin{gathered} a + d + e = 0 \\ a + b + c - 3d - e = 0 - 2a - b - e = 0 \end{gathered} \qquad (1.2)$$

This set of equations must be solved. Any solution of these equations will result in a dimensionless Π term. From matrix algebra, the number of independent solutions of a set of simultaneous equations equals the number of variables for the equation set minus the rank of the coefficient matrix. The coefficient matrix becomes: (It is the array of numbers which multiply the variables a, b, c, d and e.)

$$[C] = \begin{bmatrix} 1 & 0 & 0 & 1 & 1 \\ 1 & 1 & 1 & -3 & -1 \\ -2 & -1 & 0 & 0 & -1 \end{bmatrix} \qquad (1.3)$$

The rank of a matrix is defined as the order of the largest non-zero determinant that can be constructed from the rows and columns of the matrix. For the dimension matrix of this example, one of the 10 possible 3x3 determinants is

$$\begin{bmatrix} 0 & 0 & 1 \\ 1 & 1 & -1 \\ -1 & 0 & -1 \end{bmatrix} \qquad (1.4)$$

Therefore, the rank of the matrix is *3*. Applying the rule stated above: The number of independent solutions equals the number of system variables, *5*, minus the rank of the dimension matrix, *3*. This gives two Π terms. The other three are expressed in terms of the other two, which are called excess variables.

$$\begin{aligned} a &= -d - e \\ b &= -2a - e = 2d + 2e - e = 2d + e \\ c &= 3d + e - a - b = 2d + e \end{aligned} \qquad (1.5)$$

Values can be chosen for *d* and *a* to solve for *a, b* and *c*. It makes it simple to choose *d=1* and *e=0,* resulting in *a=-1, b=2, and c=2;* then choose *d=0* and *e=1, a=1, b=1,* and *c=1*. These two sets of values can now be substituted back, resulting in two independent Π terms.

$$\begin{aligned} \pi_1 &= F^{-1}v^2D^2p^1 \\ \pi_2 &= F^{-1}v^1D^1p^1 \\ \pi_3 &= \frac{\pi_1}{\pi_2} = \frac{vDp}{v} \end{aligned} \qquad (1.6)$$

π_3 is actually the familiar Reynolds number. Any two of these three Π terms is a complete set. π_1 could be selected for calculation of the drag force as a function of the object's diameter, velocity, and liquid density. π_3 could determine the conditions at which nonlinear flow past the object would exist.

1.2.2 Equivalent Half-Order Fractal Example[9]

Many biofractal algorithms and processes are modelled using LC and RC circuits. Ionic flow, which is involved in the modelling of proton exchange membrane fuel cells (PEMFC) may work as a powerful tool in the development and widespread testing of alternative energy sources in the next decade [9], where biofractal controllers will be used to control these complex systems. The dynamic model of PEMFC, is taken from the work of Iftikhar, 2006 [9], where the originality of which lays on the use of non-integer derivatives to model diffusion phenomena. The biofractal model has the advantage of having least number of parameters while being valid on a wide frequency range and allows simulating an accurate dynamic response of the PEMFC. In the Iftukhar model, the fuel cell is represented by an equivalent circuit, whose components are identified with the experimental technique of electrochemical impedance spectroscopy (EIS), and its overall relevance is validated by comparing model simulations and laboratory experiments. The dynamic response derived from this fractional model is studied and validated experimentally using dimensional analysis, as shown in the next section.

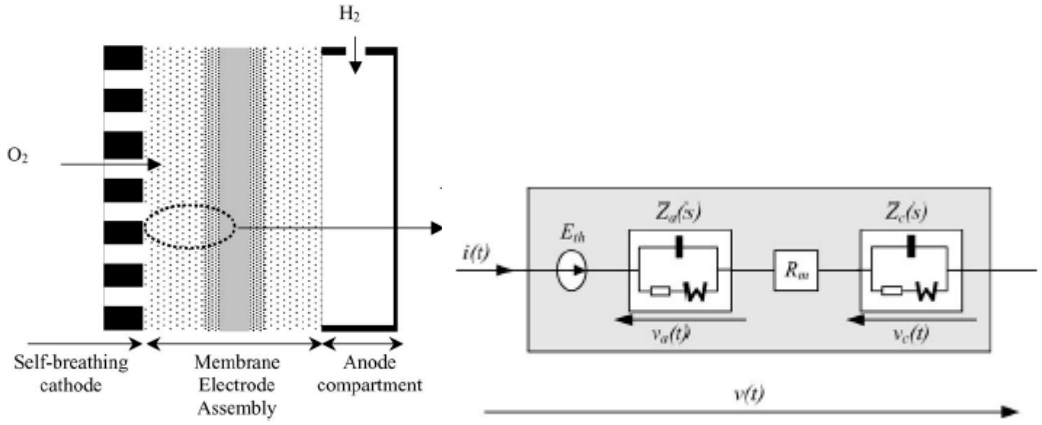

Figure 1.1 a)Proton Exchange Membrane Fuel Cell (PEMFC)[9] b) Equivalent Electrical Circuit for Modelling PEMFC[9]

In Figure 1.1, the total impedance of the electrode is [9] given by the half-order fractal transfer function as

$$Z_{\text{electrode}}(s) = \frac{1}{\frac{1}{Z_{fk}(s)} + sC_{\text{dl}}^{\text{eff}}} \tag{1.7}$$

$$Z_{fk}(s) = R_{tk} + Z_{Wk}(s) = R_{tk} + \frac{A_k(j)}{\sqrt{1 + s\tau_k}}$$

And R_{tk} is the charge transfer resistance, taken at the stationary operating point.

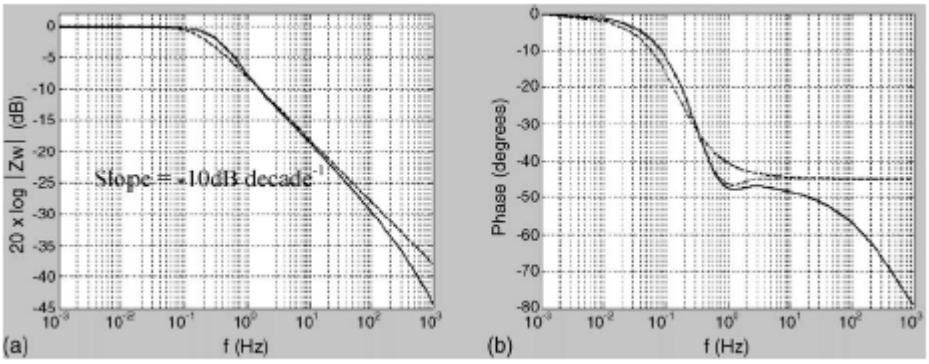

Fig. 1.2 Comparison of Electrode impedance, analytical expression (····), classical model using 20 RC cells (—), fractional model (- - -). (a) Variation of gain of impedance. (b) Variation of phase. [9]

1.2.3 Creating Scalable Dynamic Models Example[8,12]

To effectively model the dynamics of nonlinear systems, we need to form fractal expressions that are scalable, this is done by using Dimensional Analysis on the dynamic expressions. Looking at the LC circuit for "scalability, it is necessary to determine how the instantaneous current of a series LC circuit is influenced by

the voltage, inductance, and capacitance. The coefficient matrix is:

Variable	*C*	*L*	*E*	*i*	*t*
kg	– 1	1	1	0	0
m	– 2	2	2	0	0
s	4	– 2	– 3	0	1
A	2	– 2	– 1	1	0

Table 1.1: Coefficient Matrix for LC Circuit

Columns 3, 4 and 5 of rows 1,3 and 4 form a non-zero determinant. The rank of the matrix is three and the number of Π terms is two. Choosing *a* and *b* as the excess variables, then *c*, *d*, and *e* become:

$$\begin{aligned} c &= +a - b \\ d &= -a + b \\ e &= -a - b \end{aligned} \quad (1.8)$$

The solution matrix becomes:

Variable	*C*	*L*	*E*	*i*	*t*
π_1	1	0	– 1	– 1	– 1
π_2	0	1	– 1	1	– 1

Table 1.2: Solution Matrix for LC Circuit

Then $\pi_1 = \frac{CE}{it}$, $\pi_2 = \frac{Li}{Et}$, and likewise $\pi_3 = \sqrt{\pi_1 / \pi_2} = \sqrt{\frac{C}{L}}(\frac{E}{i})$. This gives the maximum current I, as a scalable, and is similar to the results obtained form the conservation-of-energy principle, where I=v $\sqrt{C/L}$. Or, another term is generated if $\pi_3 = \frac{1}{\sqrt{\pi_1 \cdot \pi_2}} = \sqrt{\frac{1}{LC}} \cdot t$, where classically, the angular frequency ω, is known to be $\sqrt{\frac{1}{LC}}$. Identical to the results obtained by classical network analysis[10].

1.2.4 Dimensional Formula, Symbols and Units [8]

Quantity, Symbol	Dimensional Formula
Kinematic Quantities	
Time Interval, t	[T]
Velocity, v	**$[LT^{-1}]$**
Quantities in Mechanics	
Mass, m	**[M]**
Force, F	**$[MLT^{-2}]$**
Density, ρ	**$[ML^{-3}]$**
Viscosity, ν	**$[L^2T^{-1}]$**
Electrical Quantities	
Charge, Q	**[Q]**
Current, I	**$[QT^{-1}]$**
Voltage, V	**$[ML^2T^{-2}Q^{-1}]$**
Electric Field, E	**$[MLT^{-2}Q^{-1}]$**
Resistance, R	**$[ML^2T^{-1}Q^{-2}]$**
Capacitance, C	**$[M^{-1}L^{-2}T^2Q^2]$**
Inductance, L	**$[ML^2Q^{-2}]$**

Table 1.3. Dimensional Formula, Symbols and Units

1.3 Using Experimental Data for Integer Modelling Nonlinear Polynomial Devices – Case Example: Tunnel Diode

Many times, we do not have the complete models for nonlinear devices, but we do have experimental measurements. The tunnel diode is an example where we use a nonlinear polynomial expression to model the device for simulation. As shown in this example, the polynomial expression becomes a high order transfer function. This example shows that why we wish to use fractal expressions to simplify the modelling and simulation.

The tunnel diode is a transconductance two-terminal, *pn* junction device that has a negative resistance region in its current versus voltage characteristic. We have seen that dimensional analysis allows us to express mathematical equations in the form of dimensionless parameters, but what happens in the case where a physical phenomena is not described by exact mathematical equations? Take for instance, the characterization of the tunnel diode, which for a SPICE simulation *(GTD POLY(1))* is described by the following polynomial expression:

I(V)= -3.95510115972848E-17
+1.80727308405845E-01*C*V
-2.93646217292003E+00*C*V^2
+4.12669748472374E+01*V^3
-6.09649516869413E+02*V^4
+6.08207899870511E+03*V^5
-3.73459336478768E+04*V^6

+1.44146702315112E+05*V^7 (1.9)
-3.53021176453665E+05*V^8
+5.34093436084762E+05*V^9
-4.56234076434067E+05*V^10
+1.68527934888894E+05*V^11

Experimentally, the tunnel diode polynomial expression may be adjusted, by the use of MAPLE, with the insertion of the parameter C. As shown in Fig. 1.3, just the slight variation of C from .99 to 1.01, results in significant variations in the transconductance model of the tunnel diode.

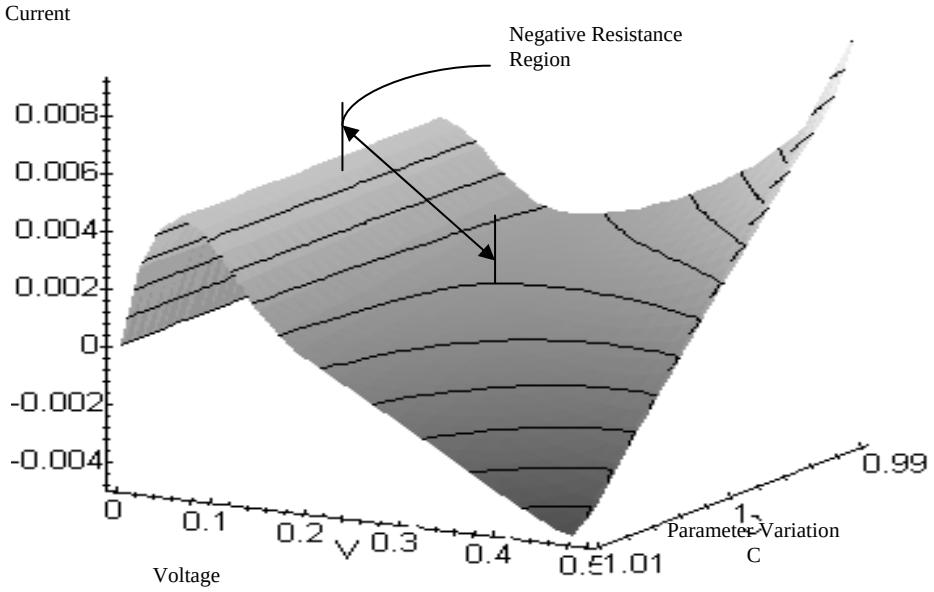

Figure 1.3 Tunnel Diode V-I Characteristics

2.0 Nonlinear Novel Organic Transistors [13]

Novel organic transistors have good potential for development of unique logic devices that don't rely on conventional electronic designs. Compared to the electrons and holes in their semiconductor counterparts, organic transistors utilize charge carriers such as electrolytes to conduct a signal. This provides the potential for custom logic built around device chemistry that can lead to reduced complexity in intricate logic implementations. This organic transistor technology is truly the target for the development of the biofractal methodology, therefore this example has in-depth detail and explanations.

2.1 Alkaline-Acid-Alkaline (LSL) Transistor [13]

Some previous researchers in the literature have attempted to incorporate organic components in semiconductor devices by using a polymer as either the gating material of a transistor, or as the semiconductor medium [13]-[17]. These devices show transistor activity, however, they can require voltages on the order of 50-100 V to operate [15]-[16]. Additionally, fabrication of these devices requires techniques that are friendly towards organic materials, which can limit additional processing of the device, due to the multitude of strong solvents and high temperatures used in traditional semiconductor device fabrication.

Development of a simple organic electrolyte diode and transistor has been shown in literature utilizing acid/alkaline chemistry. The design has acid and alkaline source chambers separated by a polymer gel. The gel allows diffusion of the electrolytes between the source chambers, but not convection. As described in previous work, the electrolyte transistors have either an acid-alkaline-acid (SLS) or an alkaline-acid-alkaline (LSL) configuration, which both have unique device characteristics. According to the literature, the SLS electrolyte transistor is a stable, amplifying device, while the LSL transistor exhibits nonlinear output current characteristics. The research performed thus far on the electrolyte transistor has been experimental measurements of steady state current values, which can take hundreds of seconds to reach [18]-[20]. So far the question of rapid transient response has not been fully explored, which is the real issue when developing novel transistors.

The LSL transistor appears to have interesting nonlinear characteristics that have the potential to lead to more rapid switching times. This example focuses on examining the complex dynamic response of the LSL polymer-electrolyte transistor (PET), utilizing the modelling program COMSOL Multiphysics. In the near future, we will incorporate the biofractal models.

To reduce confusion, the word “base” will refer to the middle acidic region of the PET, while the word alkaline will be used to reference an electrolyte of the composition BOH.

2.2 Model Definition

The polymer-electrolyte transistor has a physical design similar to a basic bipolar junction transistor. In the PET, three separate source regions of ions are connected by a polymer gel. This gel acts as a medium through which the ions are allowed to diffuse, but there is no direct convective path between the three source regions [18]-[19].

Figure 1 depicts the basic function of the PET, showing the device biased such that VE>VB>VC. The ionic species present are the alkaline BOH and the acidic HA, where B^+ is a cation and A^- is an anion. With the voltage potentials as depicted, the EB region is forward biased and the BC region is reverse biased. In a forward-biased junction, the anion and cation flow into the middle region, and allow for ionic current to flow. A reverse-biased junction is one where the H^+ and OH^- ions flow into the junction and recombine, leaving very few ions to conduct a signal [18]. With the cation flow from the emitter, though, there will be a cation concentration in the BC junction that will contribute to the total current.

2.3 Governing Equations

Ionic diffusion in the PET is described by Fick’s first law of diffusion for each ionic species. This combined with the flow of ions under an electric field produces the electrokinetic flow equation, where the

first term governs diffusive flux, and the second term governs ionic flux under an electric field:

$$\nabla \cdot (-D\nabla c - z\mu_m Fc\nabla V) = R \quad (2.1)$$

Where D is the diffusion coefficient (m^2/s), c is the concentration of the given ionic species (mol/m^3), z is the charge number (unitless), $_m$ is the ionic mobility ($mol/m \cdot s$), F is Faraday's constant (C/mol), V is the electric potential (V), and R is the reaction, or source, term ($mol/m^3 \cdot s$).

When initially determining the system of equations to govern this system, the equation for current flow due to electrons in a semiconductor material was investigated. In a semiconductor device, flux due to diffusion and drift is shown below:

$$J = qD_n\nabla n + q\mu nE \quad (2.2)$$

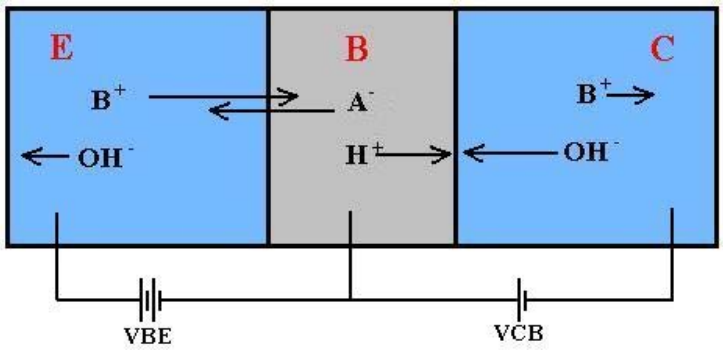

Figure 2.1. A basic PET schematic showing electrolyte migration through the emitter "E", base "B", and collector "C" under the effect of a voltage potential.

Where J is the flux of electrons (A/m^2), q is the elementary charge (C), n the density of electrons ($1/cm^3$), E the electric field (V/m), and all other units the same as equation (1) [21]. Interestingly, manipulation of this equation to apply to electrolytes moving under an electric field, where the units of flux are $mol/m^2 \cdot s$, simplifies to the equation system of equation (1).

To set up the voltage potentials in the system, the conductive media DC application is used. The governing equation for this system, shown below, is simply Ohm's law in differential equation form:

$$-\nabla \cdot d(\sigma\nabla V) = dQ_j \quad (2.3)$$

Where d is the thickness (m), is the conductivity (S/m), V is the voltage (V), and Q_j is the current (A/m^3).

2.4 Methods

The model created in COMSOL Multiphysics consists of three source regions of electrolytes, separated by a polymer, shown in figure 1.4.2. As modelled in 2D, the device is 4.5 mm long in the x-direction, by 2.3 mm wide in the y-direction. The top portion of figure 2 is the actual model built in COMSOL, including the mesh. There is a denser mesh in the regions where H^+ and OH^- recombine, due to the very high value of the reaction coefficient associated with their recombination. This high constant in the source term leads to large oscillations in concentration when the mesh is not fine enough, which produces singularities when modelling.

Thus the mesh is more refined in areas where recombination occurs.

In the bottom half of figure 2, the different regions are color coded to more clearly show the different regions of the device. The emitter and collector are both colored green to depict the source of the alkaline electrolyte, BOH. Shown in blue, the base region is the source of the acidic electrolyte, HA. The polymer gel plug is shown in orange, with enlarged areas in the three source regions due to expected gel swelling [5]. The electrodes that set up the voltage potentials are shown in silver, with one for each source region. All concentration and voltage sources are defined along the external boundary of the individual region, while bulk properties such as diffusion coefficients are defined along the subdomain.

Parameters from literature were chosen such that the acidic solution had the properties of HCl, and the alkaline solution KOH [9]. These values were picked due to their previous use in literature [18]-[19]. The properties of the modelled gel were determined from comparing diffusivity and mobility measured in literature for various electrolytes in polymer gels [13]. Concentrations and bias voltage ranges were chosen for values expected to be used during testing of a fabricated PET.

Multiple simulations were run for: i) varied salt electrolyte concentration added to the base, ii) different values of alkaline concentration (i.e. “doping”) in the emitter, iii) varied levels of the voltage VE, and iv) varied levels of the voltage VB. Simulations for (i) were performed for steady state values of ionic current using transient simulations run until a constant steady-state behavior was observed. For (ii)-(iv), transient responses for 2 s, with samples taken every 0.5 ms, were modelled to observe the times required to switch the device on, which will be important when using the PET for logic applications.

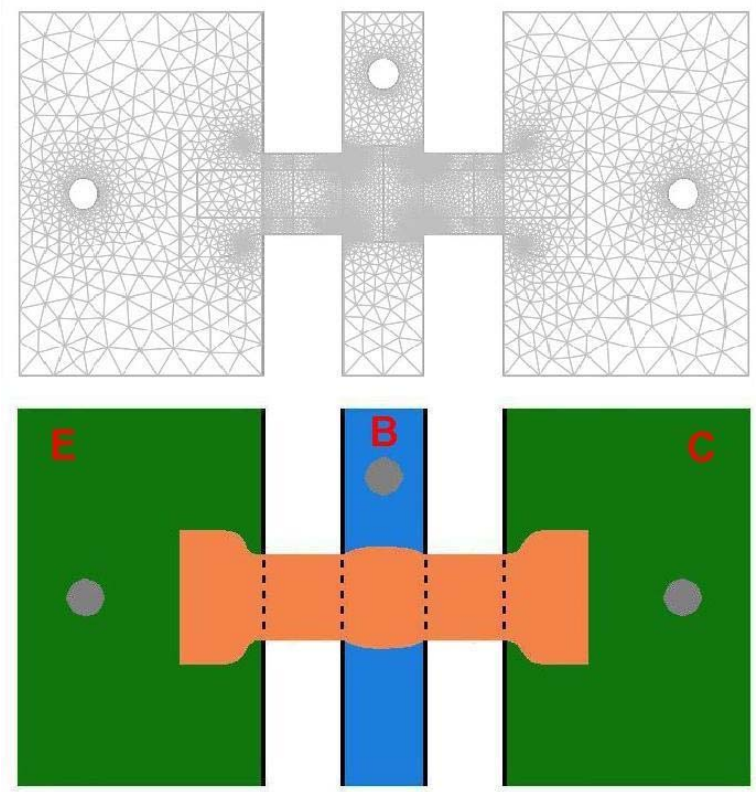

Figure 2.2. PET model showing the mesh in COMSOL (top) and the different regions colored for clarity (bottom).

2.5 Results & Discussion

Multiple simulations were run to obtain each set of data shown in this work. Convergence time to reach steady state depended on both the applied voltage, as well as the concentrations of the alkaline and acidic sources, but was on the order of tens to hundreds of seconds. Although this may seem like a long time, literature has shown that the time to reach steady state is proportional to the square of the depth of the diffusion region [20]. This implies that shrinking the device by about one order of magnitude will result in times to reach steady state of a few seconds or less.

2.5.1 Varied Electrolyte in the Base Region

Injection of charge carriers into the base region of the PET results in a noticeable change in the steady state currents. This was accomplished by adding additional salt electrolyte concentration to the base region, and observing its effect on the total current change from initial to steady state. Voltage values in the device were held constant at VE = 3.5 V, VB = 2.0 V, and VC = 0V.

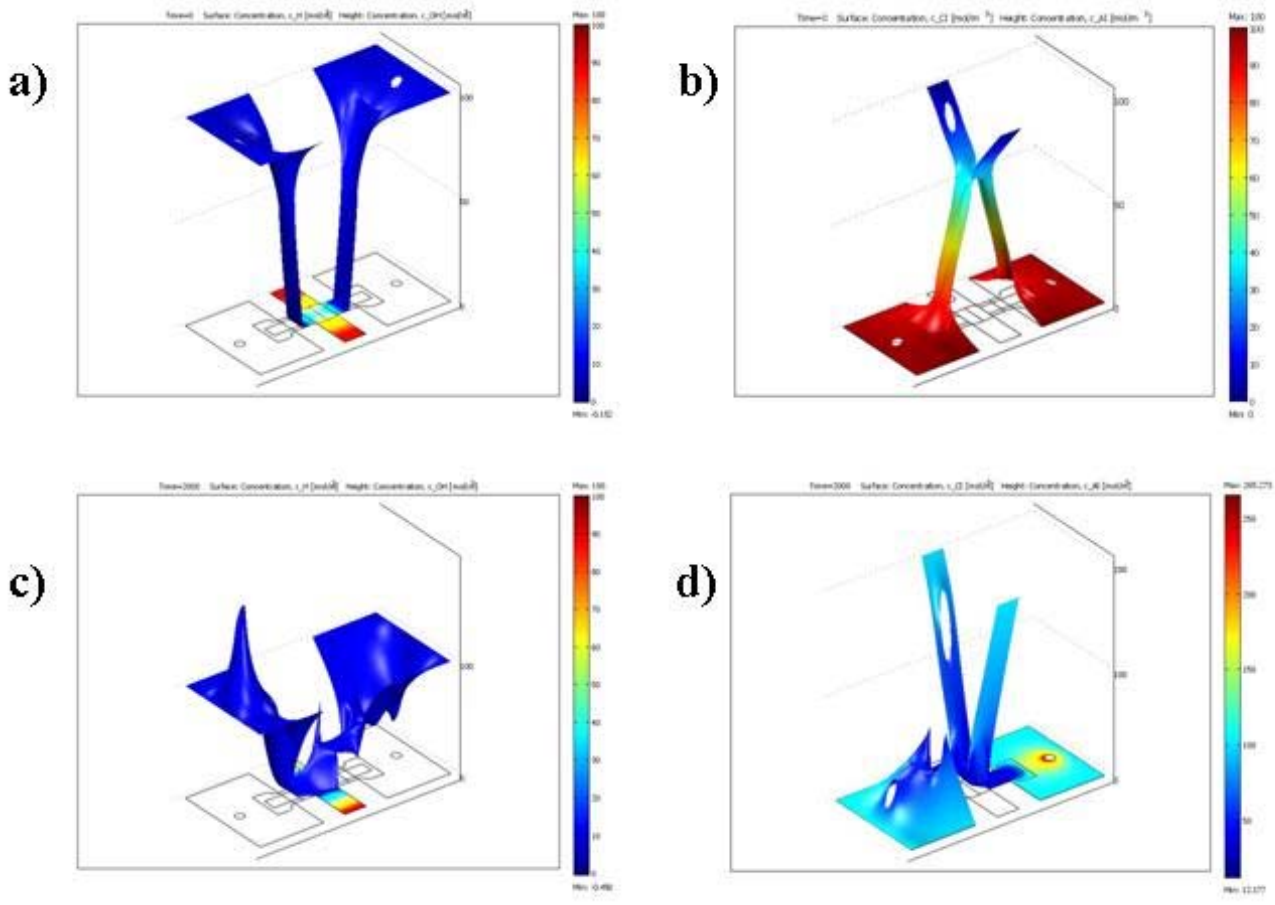

Figure 2.3. On top, results for initial value of steady state diffusion for (a) concentration H^+ color scale and OH^- height scale, (b)

concentration B^+ color scale and A^- height scale. On bottom, results for steady-state value of electrokinetic flow for (c) concentration H^+ color scale and OH^- height scale, (d) concentration B^+ color scale and A^- height scale.

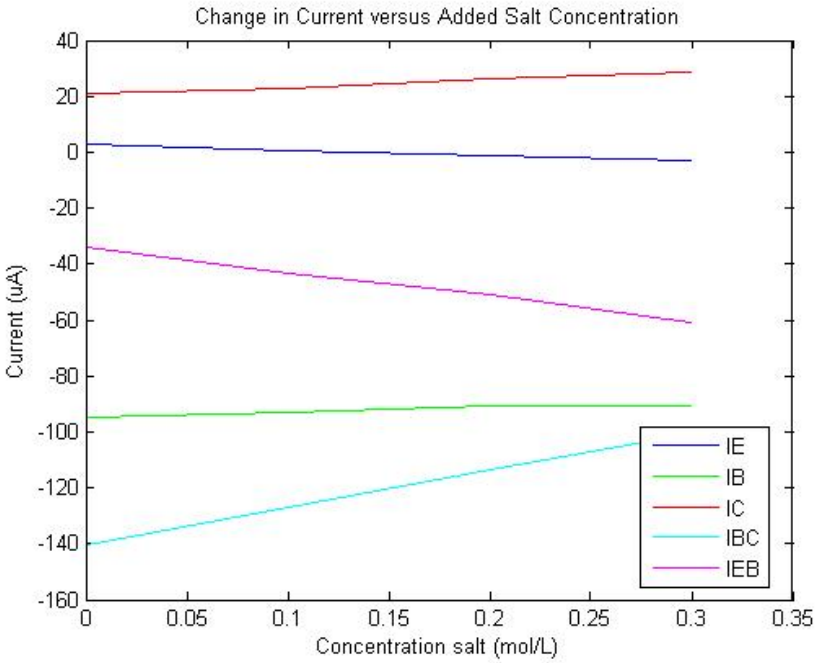

Figure 2.4. Steady-state current plot for the different regions of the device versus an increase in the concentration of salt electrolyte added to the base region of the PET.

From figure 4, the currents through the BC region of the device grow more positive with the increase of additional salt, while the currents in the EB region become more negative. This makes sense, given the voltage bias of the device, since the anion would flow towards the more positive emitter region and the cation would flow towards the more negative collector region. Depending on specific device chemistry, this property of the PET to add additional charge carriers to specific regions can be exploited to modify logic and switching points of the device, and is relatively simple to accomplish.

2.5.2 Emitter Region "Doping"

In BJTs, the emitter is typically doped more heavily with charge carriers than the collector, to allow for a very small diffusion region through the base [24]. This increases the speed of the device, since diffusion of charge carriers through the base is a speed-limiting factor.

The concentration of the alkaline source in the emitter of the PET was varied from 0.1 M to 0.4 M, and the transient current response of the device was plotted for the BC and the EB channel. From figures 5 and 6, the currents show an inverse relationship to the increased emitter doping. For increasing doping values, the BC channel current becomes more negative, while the EB channel current grows more positive.

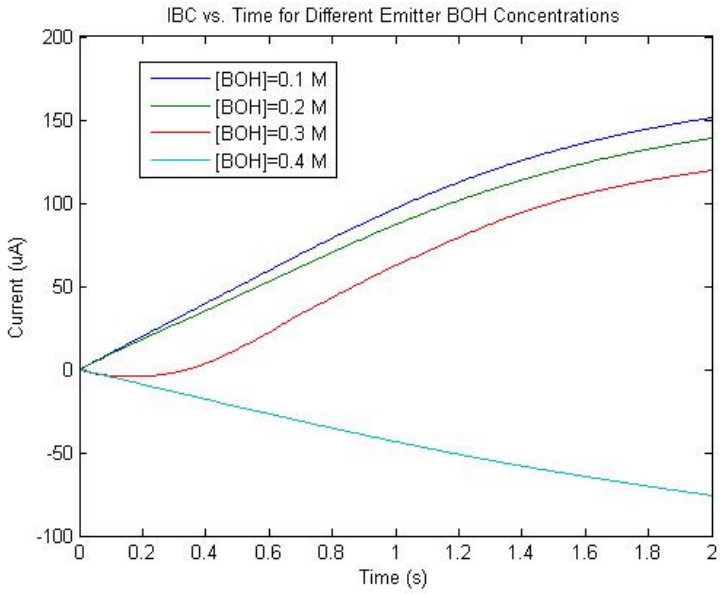

Figure 2.5. Plot of current in the BC channel versus time for different concentration doping of the alkaline source at the emitter.

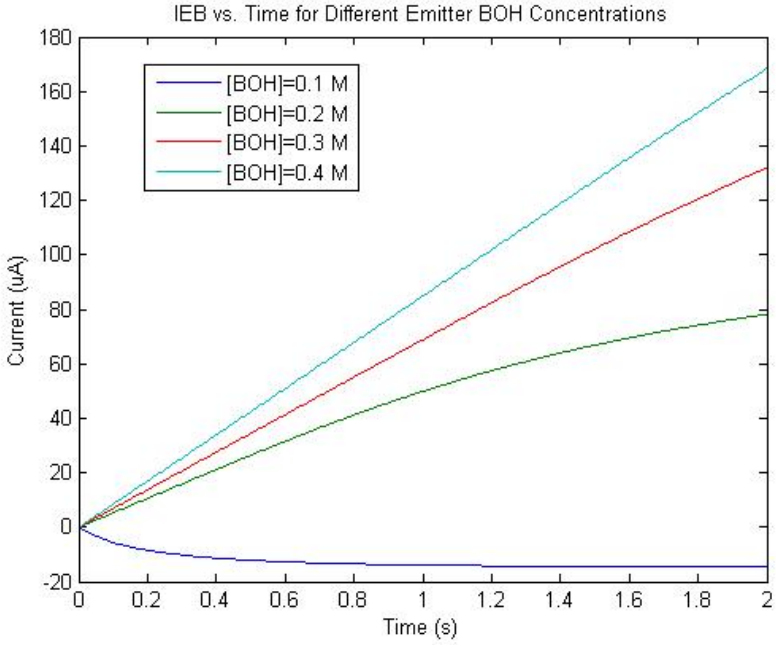

Figure 2.6. Plot of current in the EB channel versus time for different concentration doping of the alkaline source at the emitter.

From figures 2.5 and 2.6, specific device characteristics can be modified. To obtain a maximum positive current through both the EB and BC channel, an emitter doping between 0.2 M and 0.3 M would be ideal. Choosing a concentration in that range would produce a current profile most similar to a conventional BJT in the active mode. Because of the variable nature in the PET currents for different emitter doping values, a large degree of customizability is available without loss in function.

2.5.3 VE Modulation

With the PET voltage biased in common collector mode, such that VE>VB>VC=0 V, an increase in VEC above 0 V should result in an increase in current through the device, while a decrease in VEC below 0 V should lead to decreased currents. This is observed in figure 7, where more negative values of VE show a decrease in the current through the device. Although there is a residual amount of leakage current, the device exhibits transistor-like behavior, where increasing VE causes a greater flux of ions through the device.

2.5.4 VB Modulation

Similar to modulating VE, modulating VB should increase the currents in the device for values of VB > VC, while values of VB < VC should decrease the currents to a small value. This is seen from the results in figure 8, where values of VB < 0 show a very small current even at a time point of 2 s, whereas for VB > 0, a large increase in current is seen for increasing values of VB.

From figures 7 and 8, the PET shows good potential for use as an organic transistor. The ability to regulate the amount of current through the device in a manner similar to a BJT allows for a starting point in studying the possible interconnects between multiple PETs to create a logic function.

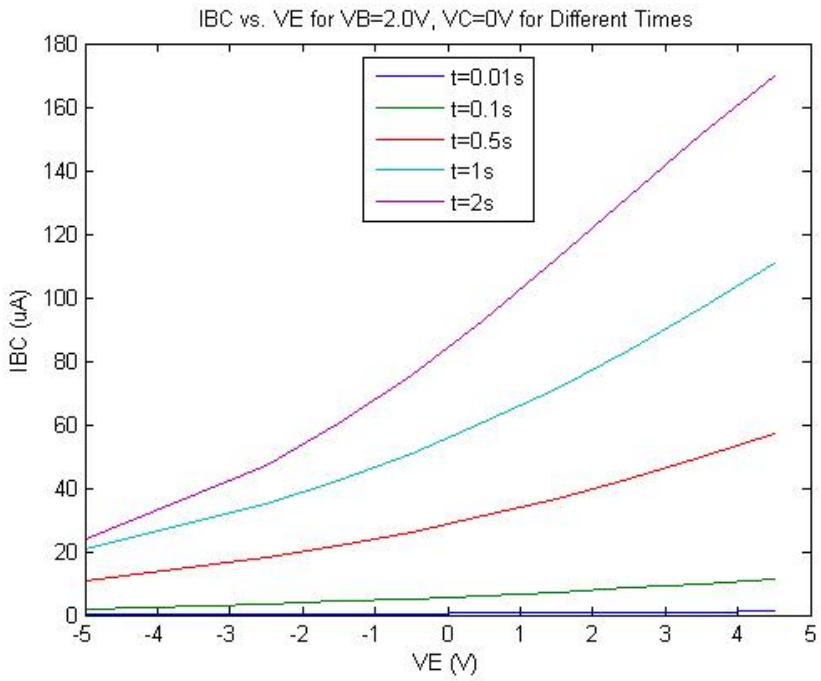

Figure 2.7. Plot of current through BC channel versus varying VE over different values of time from 0.01 s to 2 s.

This example has shown the use of COMSOL Multiphysics to model the complex chemical system of the polymer-electrolyte transistor. The PET is a good candidate for novel logic applications, due to its

transistor-like characteristics. By carefully selecting the acid/base chemistry and the composition of the polymer, specific logic can be built in to the chemistry of the device, rather than the structure. This will lead to a new domain of organic transistor design, where the transistor no longer has to mimic its semiconductor counterpart, but will operate based on new methods of logic that work well in the chemical domain. Additionally, use of multiphysics modelling applications will allow for rapid prototyping of specific device chemistry and composition, which will save time and money in the production and testing of new devices.

3.0 Half Order Fractal Element [24]

In section 2, the three dimensional diffusion equation was solved for the organic device. The one dimensional diffusion equation, leads to the implementation of a half order fractal element. The half order element (semi-infinite lossy line (Hartley and Lorenzo (1998)))[25] is based on the one-dimensional diffusion equation, Equation 3.1.

$$\frac{\partial v}{\partial t} = \alpha \frac{\partial^2 v}{\partial x^2} \tag{3.1}$$

which is depicted by a ladder of discrete resistors and capacitors as an element in Figure 3.1 a), with the impedance solution described by

$$v(t) = r\sqrt{\alpha}\,\frac{d^{-1/2}\,i(t)}{dt^{-1/2}} + \varphi_1(t) \tag{3.2}$$

and as a transfer function circuit element in Figure 3.2 b) with the Laplace expression, as given in Equation 3.3

$$\frac{v_o(s)}{v_i(s)} = -\frac{r\sqrt{\alpha}}{Rs^{1/2}} \quad . \tag{3.3}$$

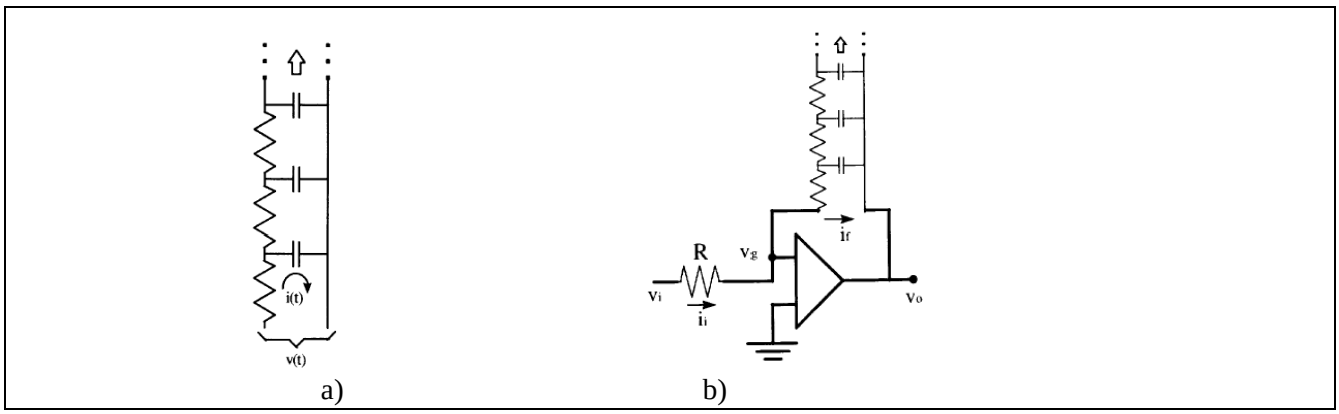

Figure 3.1 Half Order Fractal implemented as an element in a) and transfer function circuit element in b)

4.0 Fractal Order Controllers

Fractal order algorithms have been successfully used in PID controllers since 1961 as noninteger integrals [26], and more recently in 1991, [27] studied the fractal order algorithms for the control of dynamic systems, showing the superior performance of the CRONE (Commande Robuste d'Ordre Non Entier) method involving the fractal order transfer functions. Recently, Quantitative Feedback Theory has successfully been used to implement fractal order controllers, which will be the focus of Section 4.1.
The advantage of QFT is in its control for both magnitude and phase characteristics. For background information, we will define the PID controller.

In defining the PID controllers, from Wikipedia, the free encyclopedia, it's explained as the following:

Wikipedia Definition: **A proportional–integral–derivative controller (PID controller) is a generic control loop feedback mechanism widely used in industrial control systems. A PID controller attempts to correct the error between a measured process variable and a desired setpoint by calculating and then outputting a corrective action that can adjust the process accordingly.**
The PID controller calculation (algorithm) involves three separate parameters; the Proportional, the Integral and Derivative values. The Proportional value determines the reaction to the current error, the Integral determines the reaction based on the sum of recent errors and the Derivative determines the reaction to the rate at which the error has been changing. The weighted sum of these three actions is used to adjust the process via a control element such as the position of a control valve or the power supply of a heating element.
By "tuning" the three constants in the PID controller algorithm the PID can provide control action designed for specific process requirements. The response of the controller can be described in terms of the responsiveness of the controller to an error, the degree to which the controller overshoots the setpoint and the degree of system oscillation. Note that the use of the PID algorithm for control does not guarantee optimal control of the system or system stability.

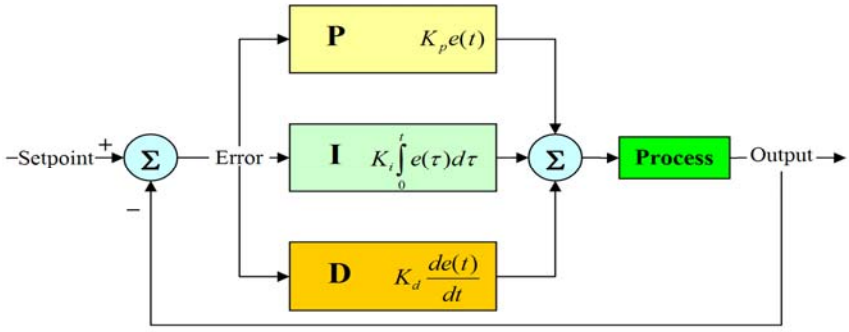

4.1 Overview of the QFT Design Technique (Incorporating the Op-Amp Component)

The QFT design technique, developed by I.M. Horowitz [5,6,7] in 1972, and extended by C.H. Houpis [8,9,10] for continuous and discrete systems, provides the necessary methodology in the design of a robust compensator for the analog-digital subcircuit. QFT provides a robust design methodology for synthesizing a compensator controller for a control system containing a plant *P* having structured parametric uncertainty. The robustness is achieved by satisfying a desired set of performance specifications and minimizing the effect of device noise (disturbance). Shown in Fig. 4.1(a) is the QFT feedback structure composed of the compensator, *G*(s), the prefilter, *F*(s), and the uncertain plant *P*(s).

The transfer function of a linear time-invariant (LTI) Op-Amp (Section 3. Half-Order Fractal for Figure 3.1b) is of the form (See Fig. 4.1):

$$P(s) = \frac{K(s - z_1)...(s - z_w)}{(s - p_1)...(s - p_n)} \qquad (4.1)$$

where $n > w$ and assuming the nondominant poles and zeros of the transfer function are at a high frequency and outside the desired bandwidth. The region of uncertainty in parameter space can be described by a set of LTI plants, i.e.:

$$P(s)=P_j(s) \quad \text{where} \quad j=1,2, \ldots, J \qquad (4.2)$$

where J represents the number of LTI plants that describe the boundary of the region of plant parameter uncertainty. The models can be reduced to the simple form shown in Fig. 4.1(b) since the nondominant pole and zeros lie outside the bandwidth of concern.

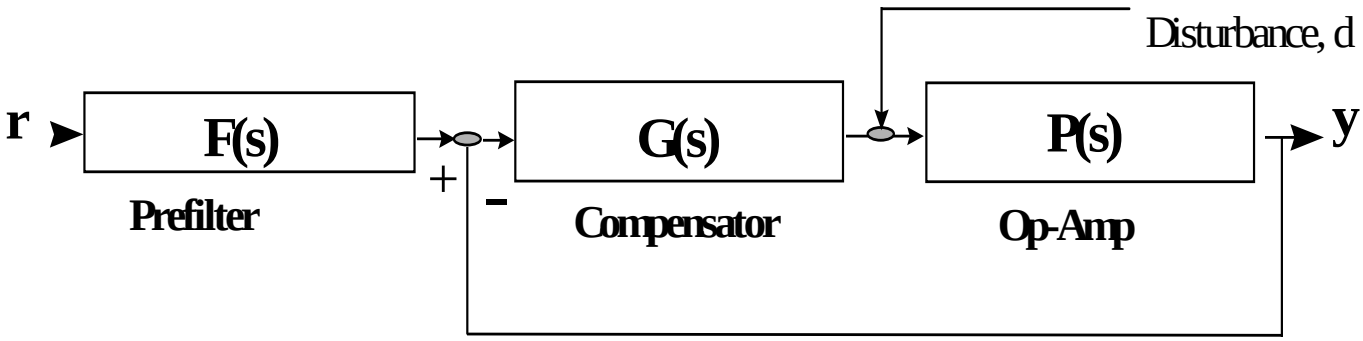

(**a**) QFT Feedback Structure

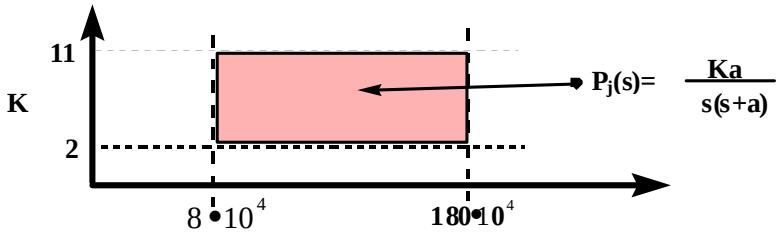

(**b**) Op Amp (Plant) Uncertainty Bounds for Dominant Pole

Figure 4.1: (a) QFT Feedback Structure, (b) Op Amp (Plant) Uncertainty Bounds for Dominant Pole

Referring to Fig.4.1(a), a multiple-input single-output (MISO) control system, the output **y(t)**:

$$\mathbf{y(t)= y_r(t) + y_d(t)} \qquad (4.3)$$

is required to track the command input **r(t)** and to reject the disturbance input **d(t)**. A MISO control system requires the design of a cascade compensator *G(s)* and of an input prefilter *F(s)*. The compensator and prefilter are designed so that the Op-Amp output response $\mathbf{y_r(t)} \approx \mathbf{y(t)}$ always lies between the upper T_{RU} and

the lower T_{RL} desired time responses and their corresponding frequency domain, respectively, bounds of Fig. 4.1 irrespective of the parametric uncertainty and where the effects of the disturbance on the output is negligible, i.e., $\mathbf{y_d(t)} \leq \alpha_p$, where α_p is the peak value of the disturbance response. The disturbance bound for a unit step input, where $\mathbf{d(t)=u_{-1}(t)}$, is denoted as $\mathbf{T_D=\alpha_p}$. Finally the prefilter must be designed to provide the desired tracking of the command input **r(t)** by the output $\mathbf{y_r(t)}$.

To facilitate the QFT design, two types of control ratios are developed from Fig. 4.1: a tracking transfer function $\mathbf{T_r(s)}$ and a disturbance transfer function $\mathbf{T_d(s)}$. Therefore, the object is to guarantee that the tracking control ratio $\mathbf{T_{dj}(s)=y_{rj}(s)/r(s)}$ always lies between $\mathbf{T_{RU}}$ and $\mathbf{T_{RL}}$ and $\mathbf{T_{dj}(s)} \leq \alpha_{\mathbf{p}}$ for all P_j in P.

Considering the Op-Amp, robust performance may be achieved by internal or external compensation techniques within the subcircuit. Internal compensation involves either the redesign of the subcircuit or modification of device parameters and components. External compensation, can be performed, without subcircuit modification by a compensator. That is, the defective Op-Amp can be replaced by a commercial off-the-shelf (COTS) Op-Amp without affecting the robust performance of the analog-digital subcircuits. A strong advantage of the external compensation technique is that existing subcircuit designs can be reused in synthesis, providing a methodology for designing complex, large scale analog-digital systems. The QFT design resulted in the following compensator and prefilter transfer functions.

$$G(s) = \frac{4 \times 10^{21}(s + 500{,}000)}{s(s + 9.0 \times 10^{8} \pm j1.2 \times 10^{9})} \qquad (4.4)$$

$$F(s) = \frac{3.6 \times 10^{13}}{s + 3.6 \times 10^{6} \pm j4.8 \times 10^{6}} \qquad (4.5)$$

Figure 4.2, shows the QFT Compensator, Filter and Plant structure of a typical commercial off-the-shelf 741 Op-Amp consisting of bipolar npn/pnp transistors. Various combinations of npn/pnp device parameters, along with variations in the frequency compensator capacitor element *CC*, were simulated using an inverting 741 Op-Amp configuration with TOTAL-SPICE. Robust performance may be achieved by internal or external compensation techniques within the subcircuit. Internal compensation involves either the redesign of the subcircuit or modification of device parameters and components. External compensation, can be performed, without subcircuit modification by a compensator.

The Op-Amp component is used for circuit design without affecting the robust performance of the fractal circuits designs in Figure 3.1. A strong advantage of the external compensation technique is that existing subcircuit designs can be reused in synthesis, providing a methodology for designing complex, large scale fractal simulation systems.

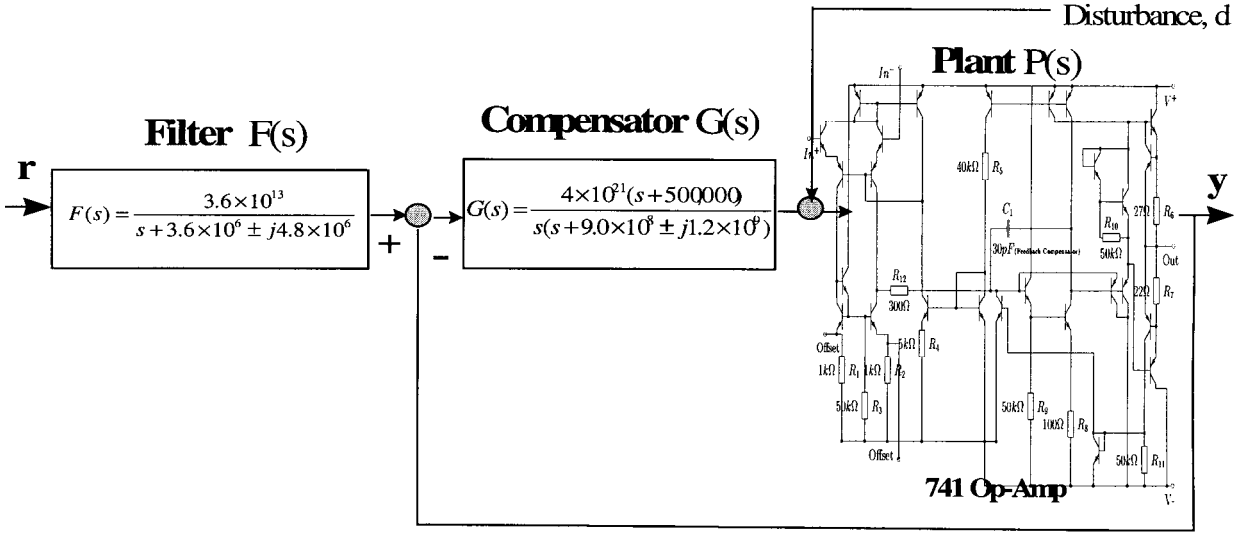

Figure 4.2. Robust Op-Amp Design using Total-Spice

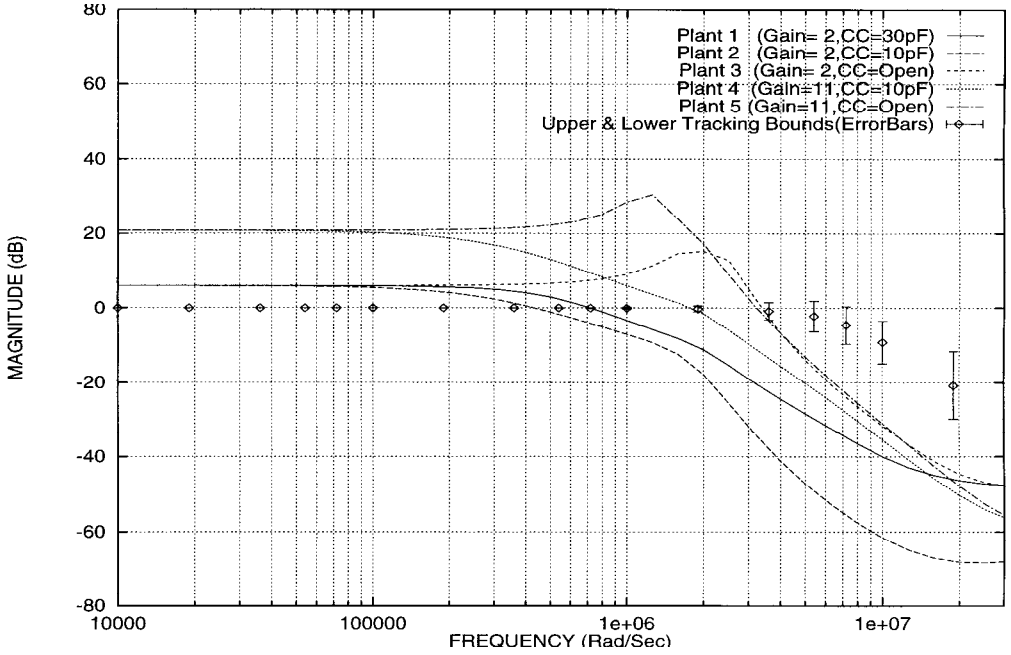

Figure 4.3. Uncompensated Op-Amp Design, shows nonlinear output variations due to component variations (Simulated with Total-Spice)

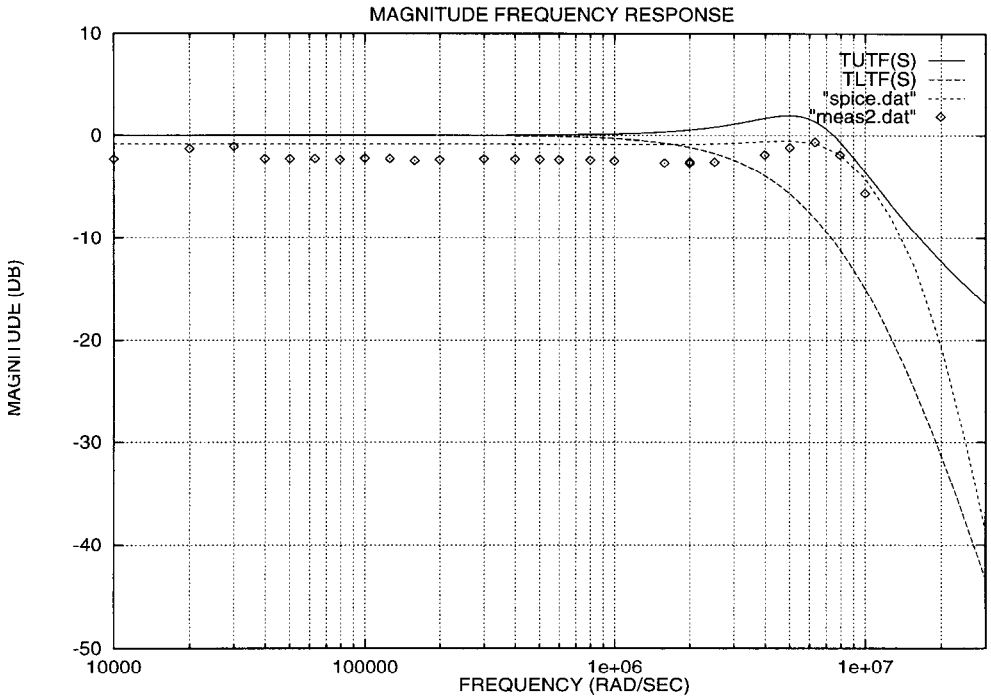

Figure 4.4 Robust Op-Amp Design (Simulated with Total-Spice)

4.2 QFT Design of a Fractal Controller [28]

The fractal controller adopted in CRONE, is the use of fractal controllers for minimizing the search space by using a minimum number of parameters, while still displaying a full frequency behavior. This idea has been used by [28] in previous works for automatic loop shaping in QFT, by using some fractal controller structures including CRONE and second order fractal structures. The purpose of section is to apply QFT for the tuning of a fractional PID controller (PIADII) of the form [28]:

$$C(s) = K_P(1 + K_I s^{-\lambda} + K_D s^{\mu}) \qquad (4.6)$$

where λ, μ are the orders of the fractional integral and derivative, respectively, in Equation 4.6. The objective is to take advantage of fractal orders in the controller C(s) and fulfill different design specifications for a set of plants describing biofractal devices, such as the organic device described in Section 2.

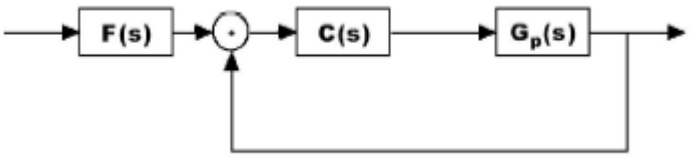

Figure 4.5 QFT Feedback Structure used for the Fractal Controller {28}

From reference [28], "Loop shaping problem in QFT is a key design step, and it consists on the shaping of the open loop gain function to a set of restrictions (or boundaries) given by the design specifications and the (uncertain) model of the plant. Although this step has been traditionally performed by hand, the use of CACSD tools (e. g. the QFT Matlab Toolbox), has made the manual loop shaping much more simple [28]. Another possibility as indicated in [28], is to use evolutionary algorithms, able to face nonlinear and nonconvex optimization problems as adopted in [29] and [30]. All these approaches have used rational integer controllers, where a low order controller gives a poor result in the control of nonlinear systems. Therefore, a very high order rational controllers needs to be used to obtain a close to optimal solution, or a fractal controller. This is a main drawback of the standard QFT automatic loop shaping techniques, since the resulting optimization problem is considerably harder as the number of parameters (directly related with the controller order) is increased, therefore the C(s) controller used in this example is Equation 3.6 and applied to the plant G(s)".

The plant is a liquid level system, and by experimental identification the transfer function model is of the form

$$G_p(s) = \frac{k}{\tau s + 1} e^{-Ls} \tag{4.1}$$

where, in addition, parameters k and T have interval uncertainty, given by k $\in$ [2,9.8] and T $\in$ [380sec, 1200 sec]. The results of this implementation [28] is shown for both an integer (L=0) and noninteger (L=5) controller

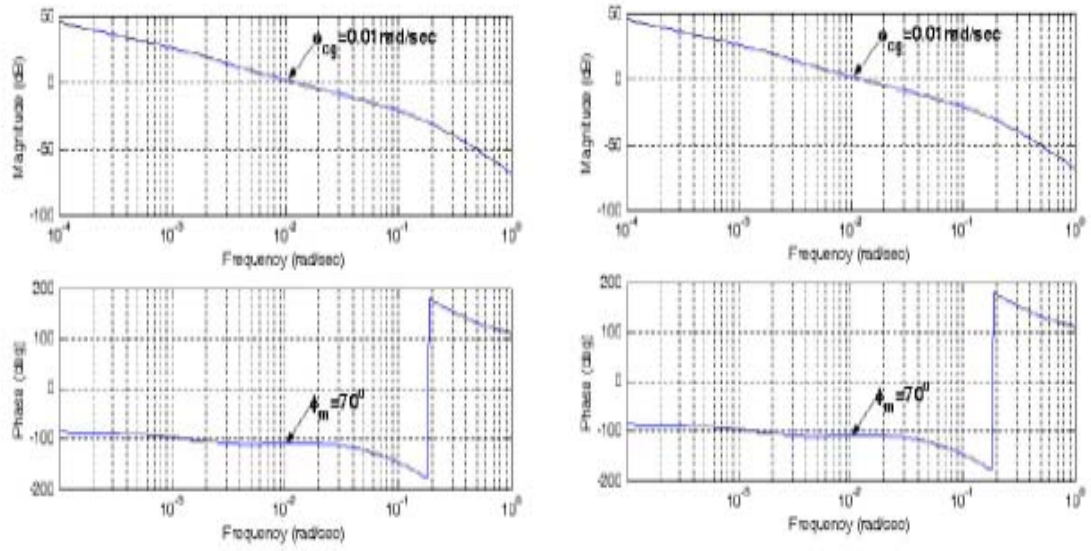

a) b)

Figure 4.6 Bode diagram of the nominal open loop for a) L=0 sec and b) L=5 sec [28]

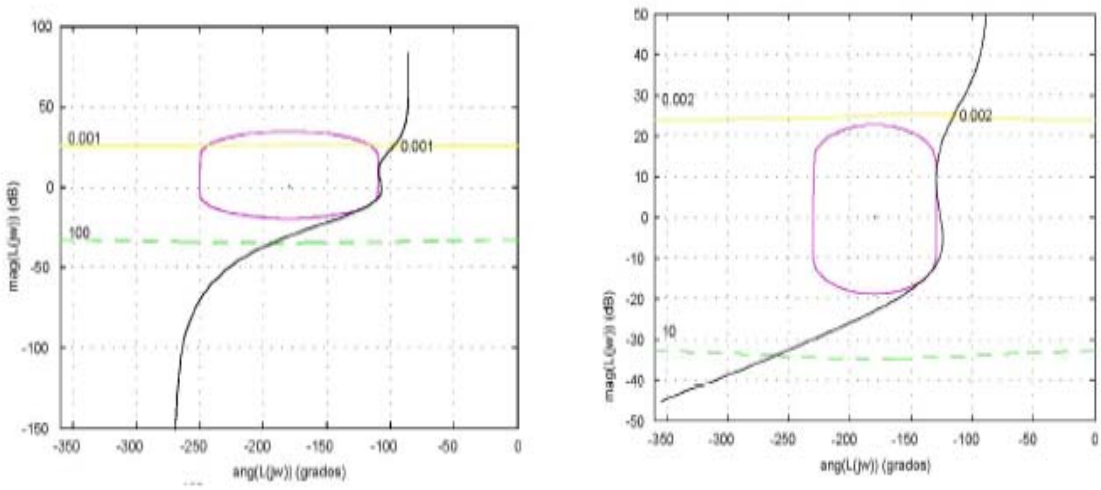

a) b)

Figure 4.7 Nichols diagram of the nominal open loop for a) L=0 sec and b) L=5 sec [28]

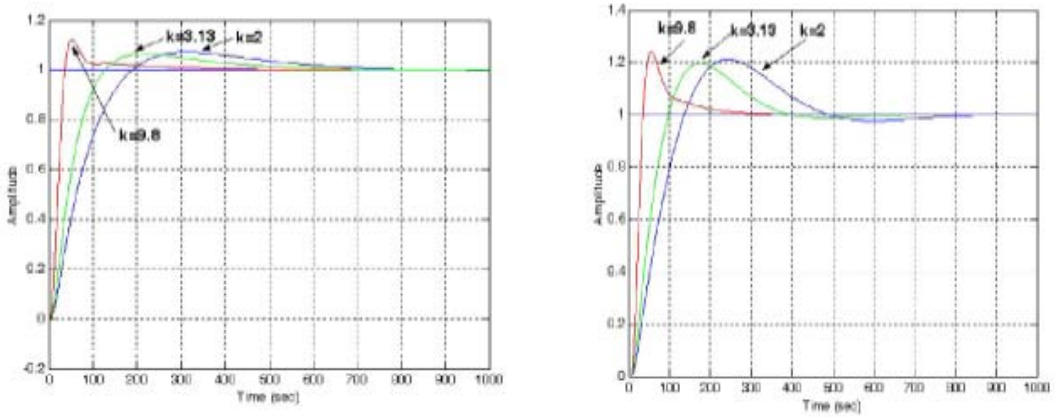

a) b)

Figure 4.8 Step response of the controlled system for a) L=0 sec and b) L= 5 sec for different values of k [28]

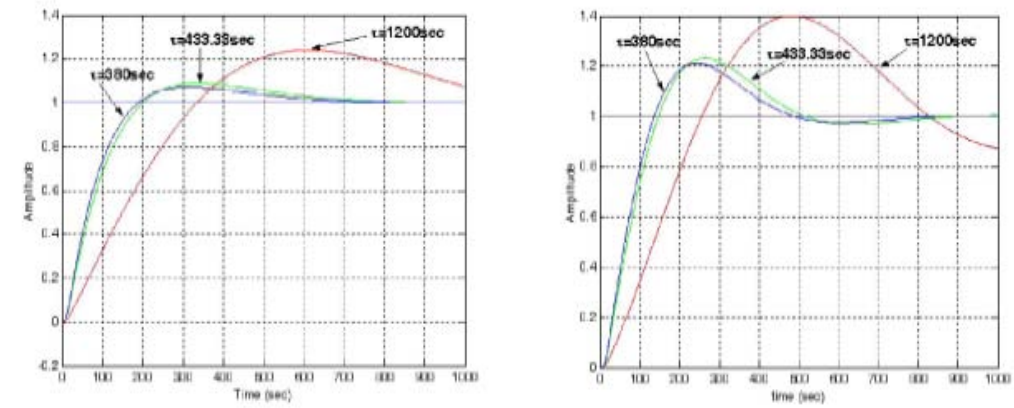

a) b)

Figure 4.9 Step response of the controlled system for a) L=0 sec and b) L=5 sec for different values of τ [28]

5.0 Summary

5.1 Enhance existing QFT approaches. For traditional electronics, fractal controllers bogs down with system complexity. Existing algorithms cannot keep pace with the exponential growth in state-space with system size of the three dimensional diffusion problems for the micro-organic biofractal systems. Yet if novel organic device capabilities such as ionic flux devices are enabled, then QFT may be able to "bootstrap" its own robustness by determining the parameters of the fractal control algorithms into geometry independent parametric search regions [31] that are both robust and power efficient.

5.2 Invent new QFT approaches. If successful, one must then ask if this approach meets micro system control needs, and if the micro system would be able to formulate its control requirements using biofractals, which are scaled by dimensional analysis. Dimensional Analysis can be applied to the electrical circuit

controller (solid-state implementation), a microfluidic sensor device and an organic biofractal system [32]. The dimensionless products can determined, and identified to classical similar results, indicating the effectiveness of Buckingham parameters in the scaling of nonlinear devices. In fabrication of organic devices, the material parameters depend on the electric and magnetic fields, where the Maxwell's equations become nonlinear, and dimensional analysis may become a valuable tool. This is similar to the situation in the nonlinear fluid dynamics example (Section 4), where the Reynolds number plays a significant part, and is an actual Π parameter. Since the system QFT topology is viewed as a form of transfer functions, parametric algebraic solutions within the frequency domain, can be generated in the form of Buckingham Π parameters related to the fractal components for future systems such as micro sensory distributed systems.

6.0 REFERENCES

[1] Oldham, K.B. & Spanier, J. (1974). *The Fractional Calculus,* Academic Press, Inc., Mathematics in Science and Engineering, Volume 111, Chapter 11.

[2] Riu, D., Reti`ere N., M. *Ivan`es, Induced currents modelling by half-order systems application to hydro- and turbo-alternators,* IEEE Trans. Energy Conversion 18 (1) (2003) 94–99.

[3] Bode, H.W., *Relations between Attenuation and Phase in Feedback Amplifier Design,* Bell System Technical Journal, vol. 19, 1940, pp.421-454.

[4] Bode, *Netwvork Analysis and Feedback Amplifier Design*. Van Nostrand, NY, 1945.

[5] Horowitz, I. *Quantitative Feedback Design Theory - QFT (VoL 1*). QFT Press. Boulder, Colorado, USA, 1993.

[6] Bridgeman, P.W.,*Dimensional Analysis, New Haven*: Yale University Press, 1931.

[7] Houpis, C.H. and Lamont, G.B., *Digital Control Systems*, McGraw-Hill Book Company, 2nd edition, 1992.

[8] Massey, B.S. *Measures in Science and Engineering: Their Expression, Relation and Interpretation*, Ellis Horwood Limited, 1986

[9] Iftikhar, M.U, Riu, D., Druart, F., Rosini, S. Bultel, Y., Retiere, N., *Dynamic modelling of the Proton Exchange Membrane Fuel Cell using Non-Integer Derivatives*, Journal of Power Sources 160 (2006), 1170-1182.

[10] Sedra. A.S. and G.W. Smith, G.W., *SPICE for Microelectronic Circuits*, Saunders College Publishing, 3rd Edition, 1992.

[11] Middendorf, W.H., *Design of Devices and Systems*, Marcel Dekker, Inc., 1990.

[12] Ewing, R.L. and Houpis, C.H., *TOTAL-PC User's Manua*l, Air Force Institute of Technology, 1997.

[13] Hollenbeck, M.C., Abdel-Aty-Zohdy, H., Brower, R., Ewing, R. and Stevens, K., *Dynamic Response Characteristics of a Novel Electrolyte Transistor, COMSOL Conference*, October 2007, Boston, MA.

{14] Lin, F. and M. Lonergan,, *Gate electrode processes in an electrolyte-gated transistor: Non-Faradaically versus Faradaically coupled conductivity modulation of a polyacetylene ionomer, Appl. Phys. Lett.*, **vol. 88**, no. 133507, pp. 1-3, (2006)

[15] Lin, Y. Li, C. Yeh, S,. Chung, L,. Huang, Wen, T., and Wang, Y. *Organic thin film transistor by using polymer electrolyte to modulate the conductivity of conjugated polymer, Appl. Phys. Lett.*, **vol. 89**, no. 223518, pp.1-3, (2006)

[16] Manunza, I. and Bonfiglio, A. *Pressure sensing using a completely flexible organic transistor, Biosensors and Bioelectronics*, **vol. 22**, pp. 2775-2779, (2007)

[17] Panzer, M.J., Newman, C.R. and Frisbie,C.D. *Low-voltage operation of a pentacene field-effect transistor with a polymer electrolyte gate dielectric, Appl. Phys. Lett.*, **vol. 86**, no. 103503, pp. 1-3, (2005)

[18] Hegedus, L.,Kirschner, N., Wittmann, M., Simon, P.,and Noszticzius, Z., *Nonlinear effects of electrolyte diodes and transistors in a polymer gel medium, CHAOS*, **vol. 9,** no. 2, pp. 283-297 (1999)

[19] Hegedus, L.,Kirschner, N., Wittmann, M. and Noszticzius, Z., *Electrolyte Transistors: Ionic Reaction-Diffusion Systems with Amplifying Properties, J. Phys. Chem. A*, **vol. 102**, pp. 6491-6497, (1998)

[20] Lei, M., Ziaie, B., Nuxoll, E., Ivan, K., Noszticzius, Z., and Siegel, R.A., *Integration of Hydrogels with Hard and Soft Microstructures, J. Nanosci. Nanotechnol.*, **vol. 7**, pp. 780–789, (2007)

[21] Sze, S.M. *Modern Semiconductor*, pp. 14-18. John Wiley & Sons, New York (1998)

[22] Peppas,N.A., and Wright, S.L.,*Drug diffusion and binding in ionizable interpenetrating networks from poly(vinyl alcohol) and poly(acrylic acid), European Journal of Pharmaceutics and Biopharmaceutics*, **vol. 46**, pp. 15-29, (1998)

[23] Angelo,E.A., Jr., *Electronics: BJTs, FETs, and Microcircuits*, pp. 213-222, McGraw-Hill Book Company, New York (1969)
[24] Lorenzo, C.F. and Hartley, T.T., *Initialization, Conceptualization, and Application in the Generalized Fractional Calculus*, NASA/TP--1998-208415
[25] Hartley, T.T.; and Lorenzo, C.F.: Insights into the Initialization of Fractional Order Operators Via Semi-Infinite Lines. NASA TM-208407, 1998.
[26] Manabe, S., *The Non-Integer Integral and its Application to Control Systems, ETJ of Japan*, vol. 6, no. 3-4, 1961, pp. 83-87.
[27] Oustaloup, A., *La Commande CRONE: Commande Robuste d'Ordre Non Entier*, Hermes, Paris, 1991.
[28] Cervera, Joaquin, Banios, Alfonso, Monje, Concha A., Vinagre, Blas M., *Tuning of Fractional PID Controllers by Using QFT*, 32nd Annual Conference of the IEEE Industrial Electonics Society, Paris, France, November 7-10,2006, p 5402-5406
[29] Chen,W.H, Ballance, D.J. and Li,Y. *Automatic Loop-Shaping of QFT using Genetic Algorithms, Center for Systems and Control, University of Glasgow*, Glasgow, UK, 1998.
[30] Bafios, R.A., and Barreiro, A., *QFT Controller Synthesis using Evolutive Strategies*, in Proceedings of the 5th International QFT Symposium on Quantitative Feedback Theory and Robust Frequency Domain Methods, Pamplona, Spain, 2001, pp. 291-296.
[31] Oldham, K.B., *Semi-integral Electroanalysis*: Analog Implementation. Analytical Chemistry, vol. 45, no. 1, Jan. 1973, pp. 39-47.
[32] Bagley, R.L. and Calico, R.A.: *Fractional Order State Equations for the Control of Viscoelastically Damped Structures*, Journal of Guidance, Control, and Dynamics, Vol. 14, No. 2, pp. 304-311, Mar.-Apr. 1991.